J. Plasma Phys. (2025), *vol*. 91, E156 © The Author(s), 2026. Published by Cambridge University Press.
This is an Open Access article, distributed under the terms of the Creative Commons Attribution licence (https://creativecommons.org/licenses/by/4.0/), which permits unrestricted re-use, distribution and reproduction, provided the original article is properly cited. doi:10.1017/S0022377825100950

Parameter optimisation design of helicon wave plasma source in High Magnetic field Helicon eXperiment

Yan Zhou[1,2], Xuemei Wu[1,2] and Tianyuan Huang[1,2]

[1]School of Physical Science and Technology, Soochow University, Suzhou, 215006, PR China
[2]Jiangsu Key Laboratory of Frontier Material Physics and Devices, Soochow University, Suzhou, 215006, PR China

Corresponding author: Xuemei Wu, xmwu@suda.edu.cn

(Received 1 September 2024; revision received 13 August 2025; accepted 27 September 2025)

Based on the High Magnetic field Helicon eXperiment (HMHX), considering parabolic distribution and Gaussian distribution of radial plasma density, the HELIC code was used to study the parameter optimisation design of a helicon wave plasma (HWP) source. Some parameters (antenna type, radio frequency, discharge gas, plasma radius, magnetic field) were selected. The results show that a half-helix antenna is the excitation antenna and a frequency of 13.56 MHz is the most commonly used power source for HMHX. Argon and nitrogen are selected as discharge gases to achieve the best effect of power deposition. In order to realise hydrogen–HWP discharge, a new antenna with plasma radius of 10.5 mm and antenna radius of 13.5 mm can be designed. For the new antenna, when the magnetic field intensity is 1000 Gs, the best discharge effect can be achieved. The results of this paper can provide guidance for the design of a plasma source for HWP discharge under different conditions in the future.

Key words: plasma simulation, plasma devices

1. Introduction

Helicon wave plasma (HWP) source, as a revolutionary technology in the field of low-temperature plasmas, has been known for its high density (Carter *et al*. 2002), high ionisation efficiency (Batishchev *et al*. 2009), low electron/ion temperature, no electrode contact (avoiding electrode erosion and instability (Goulding, Caughman & Rapp 2017)) and flexibility of external operational parameters (wide range adjustment of magnetic field, air pressure and frequency (Shinohara 2018)). It continues to lead the development of high-efficiency plasma generation technology.

The HWP discharge can be classified into three typical working modes based on the configuration of magnetic field strength and radio-frequency (RF) power: it presents a capacitive coupling mode (E mode) in the low-magnetic-field–low-power range; an inductive coupling mode (H mode) under medium parameter conditions;

https://doi.org/10.1017/S0022377825100950 Published online by Cambridge University Press

and a helicon-wave-dominant mode (W mode) when combined with high magnetic field and high power. As the RF power and axial magnetic field gradually increase, the plasma working mode will undergo a transition from E mode to H mode to W mode. At low RF powers and low magnetic fields, HWP discharge cannot realise the helicon wave mode at all. At high RF powers and high magnetic fields, it can realise the helicon mode with helicon blue core formation (Ellingboe & Boswell 1996; Thakur, Brandt & Cui 2015; Chang, Caneses & Thakur 2022; Cui, Zang & He 2024). It is precisely because of the existence of this mode transformation, compared with traditional capacitive coupled plasma (CCP) and inductive coupled plasma (ICP) sources, that HWP sources can achieve a density leap of 1–2 orders of magnitude, which is attributed to their unique wave–particle energy coupling mechanism (Chen 2015).

In recent years, the advantages of HWP sources have been widely utilised by scholars in various fields, including thin-film deposition (Chen, Bagnall & Koh 1998; Yerokhin, Nie & Leyland 1999; Gallo, Fedorczak & Elmore 2017), wall retention cleaning in tokamaks (Huang *et al*. 2017; Huang *et al*. 2018), plasma propulsion (Charles *et al*. 2009; Shinohara *et al*. 2014; Takahashi *et al*. 2019) and toroidal current drive (Wang, Wi & Kim 2017; Li *et al*. 2020). In addition, due to its superior discharge characteristics compared with traditional CCP and ICP, the HWP can generate higher plasma density and decrease the processing time in the semiconductor etching process. However, it has not yet been accepted by the semiconductor industry, which is also a difficult problem that needs to be urgently overcome in the industrial application field of HWP (Chen 2015). For different applications, it is particularly important to perfect HWP discharge experiments. The HWP source determines the state and form of the HWP discharge. According to different research objectives, different HWP sources need to be designed to meet the experimental requirements. In order to deal with large-scale material handling and high-power plasma propulsion, it is necessary to design a large-radius antenna for HWP discharge to generate a larger volume of plasma (Chang *et al*. 2018). In tube coating experiments, it is necessary to design an HWP antenna with a small radius to generate plasma with a sufficient radius to pass through the tube base (Sun, Yan & Ji 2018; Bakeev *et al*. 2023).

In a review study (Chen 2015; Shinohara 2018; Chang, Boswell & Scime 2024), it was presented that the HWP source has evolved from miniaturised thruster applications (such as SHD (Kuwahara, Mishio & Nakagawa 2013), with a diameter as small as 0.3 cm) to large-scale basic research devices (such as LHPD (Shinohara & Tanikawa 2004, 2005; Tanikawa & Shinohara 2006), with a diameter of 73.8 cm, a length of 486 cm and the world's largest volume of 2.1 m^3). The high diversity in size and configuration of HWP sources is of great significance for the study of new HWP sources.

Designing HWP sources of different sizes requires a significant investment of time and money, as it is not feasible to rely on trial and error by continually creating new antennas. Therefore, it is crucial to determine the optimal parameters of antennas under various experimental conditions through numerical simulation. In recent years, there has been substantial progress in the numerical simulation of HWP. The HELIC code (Arnush & Chen 1998) conducts theoretical analysis of electromagnetic fields to calculate the energy deposition of helicon wave (H wave) and Trivelpiece–Gould wave (TG wave), as well as the distribution of electric, magnetic and current fields. The ANTENA2 code (Mouzouris *et al*. 1996) utilises collision mechanisms and Landau damping heating mechanisms to compute the electromagnetic field and

https://doi.org/10.1017/S0022377825100950 Published online by Cambridge University Press

power deposition in plasmas. The SPIREs code (Melazzi *et al*. 2012) employs the FDTD algorithm to efficiently solve electromagnetic field problems and power deposition problems in cylindrical plasmas. The ADAMANT code (Melazzi *et al*. 2015) uses the MOM algorithm to investigate antenna geometry and its impact on power deposition. These codes serve as valuable computational tools for designing HWP sources.

The HELIC code is able to match the boundary conditions quickly because of its unique solution method, which can significantly reduce calculation costs. Therefore, based on the High Magnetic field Helicon eXperiment (HMHX), this paper selected the HELIC code as the calculation tool to simulate the experimental parameters, to analyse the effects of antenna type, RF and discharge gas on power deposition of HWP discharge and to determine the optimal discharge parameters for the subsequent optimisation of antenna size. In addition, in order to complete a hydrogen–HWP discharge, antennas of different sizes are designed for numerical simulation, in order to obtain the optimal power deposition effect under the discharge condition of hydrogen. The research in this paper has certain guiding significance for the optimisation of HWP sources on HMHX and the development of related physical experiments.

2. Theoretical formula and calculation model

2.1. *Theoretical formula*

The HELIC code uses specific boundary conditions to solve six radially coupled differential equations (Li *et al*. 2020*a*,*b*; Zhou, Huang & Wu 2024):

$$\frac{\partial E_\varphi}{\partial r} = \frac{im}{r}E_r - \frac{E_\varphi}{r} + i\omega B_z, \tag{2.1}$$

$$\frac{\partial E_z}{\partial r} = ikE_r - i\omega B_\varphi, \tag{2.2}$$

$$i\frac{\partial B_\varphi}{\partial r} = \frac{m}{r}\frac{k}{\omega}E_\varphi - \frac{iB_\varphi}{r} + \left(P - \frac{m^2}{{k_0}^2 r^2}\right)\frac{\omega}{c^2}E_z, \tag{2.3}$$

$$i\frac{\partial B_z}{\partial r} = -\frac{\omega}{c^2}iDE_r + \left(k^2 - {k_0}^2 S\right)\frac{E_\varphi}{\omega} + \frac{m}{r}\frac{k}{\omega}E_z, \tag{2.4}$$

$$B_r = \frac{1}{k_0 c}\left(\frac{m}{r}E_z - E_\varphi\right), \tag{2.5}$$

$$E_r = \frac{D}{S}iE_\varphi + \frac{kc}{k_0 S}B_\varphi - \frac{m}{r}\frac{c}{k_0 S}B_z, \tag{2.6}$$

where B_r, B_φ and B_z are radial, angular and axial induced magnetic fields, E_r, E_φ and E_z are radial, angular and axial induced electric fields, k is axial mode number, ω is wave frequency and $k_0 = \omega/c$ with c the speed of light. Also,

$$S = 1 - \sum_\alpha \frac{\omega + iv_\alpha}{\omega}\frac{{\omega_{p\alpha}}^2}{(\omega + iv_\alpha)^2 - {\omega_{c\alpha}}^2}, \tag{2.7}$$

$$D = -\sum_\alpha \frac{\omega_{c\alpha}}{\omega}\frac{\omega_{p\alpha}}{(\omega + iv_\alpha)^2 - \omega_{c\alpha}}, \tag{2.8}$$

$$P = 1 - \sum_\alpha \frac{{\omega_{p\alpha}}^2}{\omega(\omega + iv_\alpha)}, \tag{2.9}$$

https://doi.org/10.1017/S0022377825100950 Published online by Cambridge University Press

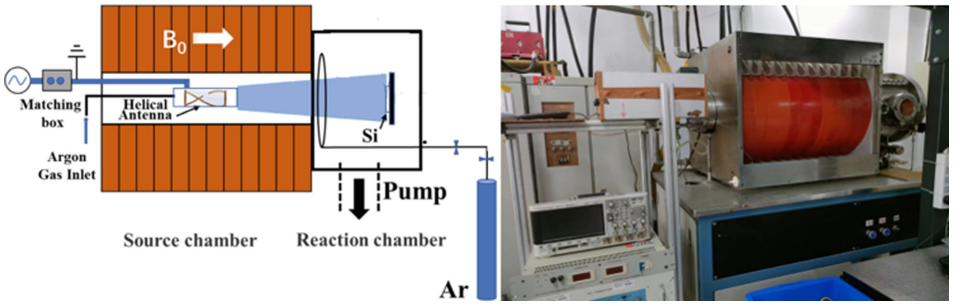


FIGURE 1. Schematic diagram and structure of HMHX.

where $\omega_{p\alpha}$, $\omega_{c\alpha}$ and υ_α are plasma frequency, plasma cyclotron frequency and effective collision frequency between particles and α is the type of particles.

As for the absorbed power of plasma, the specific plasma power spectrum function $S(k)$ is defined as

$$S(k) = \frac{1}{2} Re\left(\int \boldsymbol{E}^* \cdot \boldsymbol{J}_{\text{plasma}}\, d^3 r\right). \tag{2.10}$$

Here, $\boldsymbol{J}_{\text{plasma}}$ is the current density of plasma, which can be expressed in terms of the cold plasma tensor:

$$J_{\text{plasma}} = -i\omega\varepsilon_0 \begin{pmatrix} S & -iD & 0 \\ iD & S & 0 \\ 0 & 0 & P \end{pmatrix} \begin{pmatrix} E_r \\ E_\varphi \\ E_z \end{pmatrix}. \tag{2.11}$$

The electric field E and current density J in real space are excited by an antenna whose spectrum is $K_\varphi(k') = \delta(k' - k)$. Since S(k) is even, it can be used to simplify the calculation:

$$p_A(k) = \left|K_\varphi(k)\right|^2 + \left|K_\varphi(-k)\right|^2. \tag{2.12}$$

Therefore, the absorbed power from k to $(k + \mathrm{d}k)$ and from $-k$ to $-(k + \mathrm{d}k)$ is

$$\begin{aligned} P(k) &= S\,(k)\; p_A\,(k) \\ &= \frac{\omega\epsilon_0}{2} \int_0^a \mathrm{Im}\{S(|E_r|^2 + |E_\varphi|^2) + P|E_z|^2 + 2D\, Re\{E_r^* E_\varphi\}\} r\,\mathrm{d}r. \end{aligned} \tag{2.13}$$

Then the total absorbed power is

$$P_{abs} = 2\int_{k_{min}}^{k_{max}} P(k)\mathrm{d}k = R. \tag{2.14}$$

2.2. *Calculation model*

HMHX is independently designed and constructed by the Plasma Technology Research Center of Soochow University. A schematic diagram and structure of the device are shown in figure 1. The device uses a modular design. It can be divided into a source area (internal diameter is 228 mm, length is 800 mm) and a plasma–material interaction area (internal diameter is 400 mm, length is 400 mm). Because HMHX

https://doi.org/10.1017/S0022377825100950 Published online by Cambridge University Press

Parameter	Value
Plasma radius, R_a	14.5 mm
Antenna radius, R_b	17.5 mm
Vacuum cavity radius, R_c	114 mm
Discharge gas	Argon, nitrogen, hydrogen, helium
RF, f	2, 13.56, 20.34, 27.12, 40.68, 60 MHz
Antenna length, L_A	180 mm
Plasma density, n_{e0}	1.03×10^{13} cm^{-3}
Magnetic field, B_0	200–2000 (1185) Gs
Electron temperature, T_{e0}	3 eV
Background pressure, P_{g0}	10 mTorr
Radial step, N	49
Collisional factor	1

TABLE 1. Plasma parameters and boundary conditions.

can produce HWP of high density and energy, it can be used to study the characteristics of HWP and the interaction between plasma and material. The antenna is a right-handed helicon antenna (internal diameter is 35 mm, length is 180 mm) which is wrapped around a quartz tube with a thickness of 3 mm (Zhou *et al*. 2023). In table 1, the discharge parameters have been set. Among them, the radial step defines the mesh size of the simulation region (typically from the magnetic axis to the plasma boundary) in the radial direction. When the radial step is smaller, the computational grid becomes denser, and theoretically, the solution accuracy is higher. However, the memory and CPU time required for the calculation also increase sharply. When the radial step is larger, the calculation speed will be faster, but important physical details may be lost or inaccurate values may result. Therefore, based on some previous studies (Ping *et al*. 2019; Li *et al*. 2020*a*,*b*) on HWP using HELIC, a radial step of 49 was selected to ensure a certain balance between computational accuracy and speed. The collisional factor is a factor that artificially enhances the frequency of collisions. Excessive collisional factor can cause the resistance effect to be overly exaggerated, thereby resulting in physical distortion. However, a collisional factor that is too small will result in a resistance effect that is too weak to distinguish, making numerical solution extremely difficult.

In actual HWP discharge experimental devices, the axial magnetic field is mostly provided by electromagnetic coils or permanent magnets. This leads to subtle changes in the axial magnetic field during the actual discharge process, rather than the uniform distribution in the ideal state (D'lppolito *et al.* 2012; Hong, Li & Hajjar 2018*a*,*b*). A change in the axial magnetic field will lead to variations in the axial boundary conditions, thereby affecting the dynamic characteristics of the plasma (Thakur, Xu & Manz 2013; Vaezi, Holland & Thakur 2017*a*,*b*). In simulation studies, it can be assumed that the magnetic field does not change in the axial direction, thereby shortening the overall calculation time. Although the final result is bound to have errors compared with an actual experiment, it can basically remain consistent in the overall trend of change. In the HELIC code, the magnetic field density is uniform along the axial direction, and the density distribution of the particles is also uniform along the axial direction. The radial density can be determined by the

https://doi.org/10.1017/S0022377825100950 Published online by Cambridge University Press

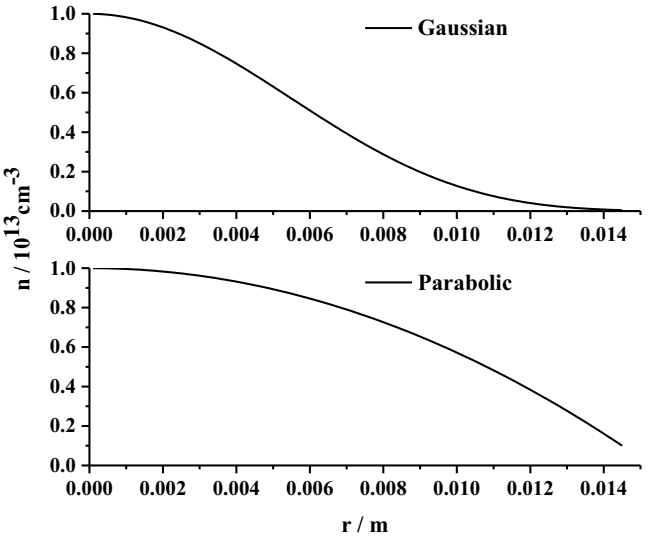


FIGURE 2. Plasma radial density distributions.

following function:

$$\frac{n}{n_{e0}} = \left[1 - \left(\frac{r}{\omega}\right)^s\right]^t, \quad \omega = \frac{R_a}{\left[1 - f_a{}^{1/t}\right]^{1/s}}, \tag{2.15}$$

where s and t are constants, f_a represents the relative density at $r = R_a$ and n_{e0} is the density at the centre of the plasma.

The radial density gradient and edge density have a great influence on the non-resonant mode conversion of H wave into TG wave and power deposition. Therefore, two common density distributions can be selected: Gaussian distribution and parabolic distribution. As shown in figure 2, these two density distributions have the same peak value on axis but different gradient in radius. The edge values of the Gaussian distribution and parabolic distribution are 0.01 and 0.1, respectively, of the peak value (Shamrai 1998).

3. Results and discussion

3.1. *Antenna type*

During the process of HWP discharge, it is essential to utilise an antenna for coupling the energy from the RF power supply to the plasma. This allows HWP to transfer energy to electrons through the TG–H coupling mode (Ping *et al*. 2019). Therefore, when designing the device, selecting the appropriate antenna type is crucial. In this study, three different antenna types were chosen: half-helix antenna (Chi, Sheridan & Boswell 1999), Boswell antenna (Charles, Boswell & Lieberman 2003) and loop antenna. The off-axis peak of the loop antenna exhibits an $m = 0$ mode structure, which differs from the $m = 1$ mode driven by the other two antennas (Jung, Park & Kim 2004). Figures 3(a1)–3(a3), respectively, illustrate the radial relative absorption power of half-helix, loop and Boswell antennas under the parabolic density distribution. By comparing figures 3(a1) and 3(a2), it can be observed that in comparison with the loop antenna, the half-helix antenna demonstrates higher

https://doi.org/10.1017/S0022377825100950 Published online by Cambridge University Press

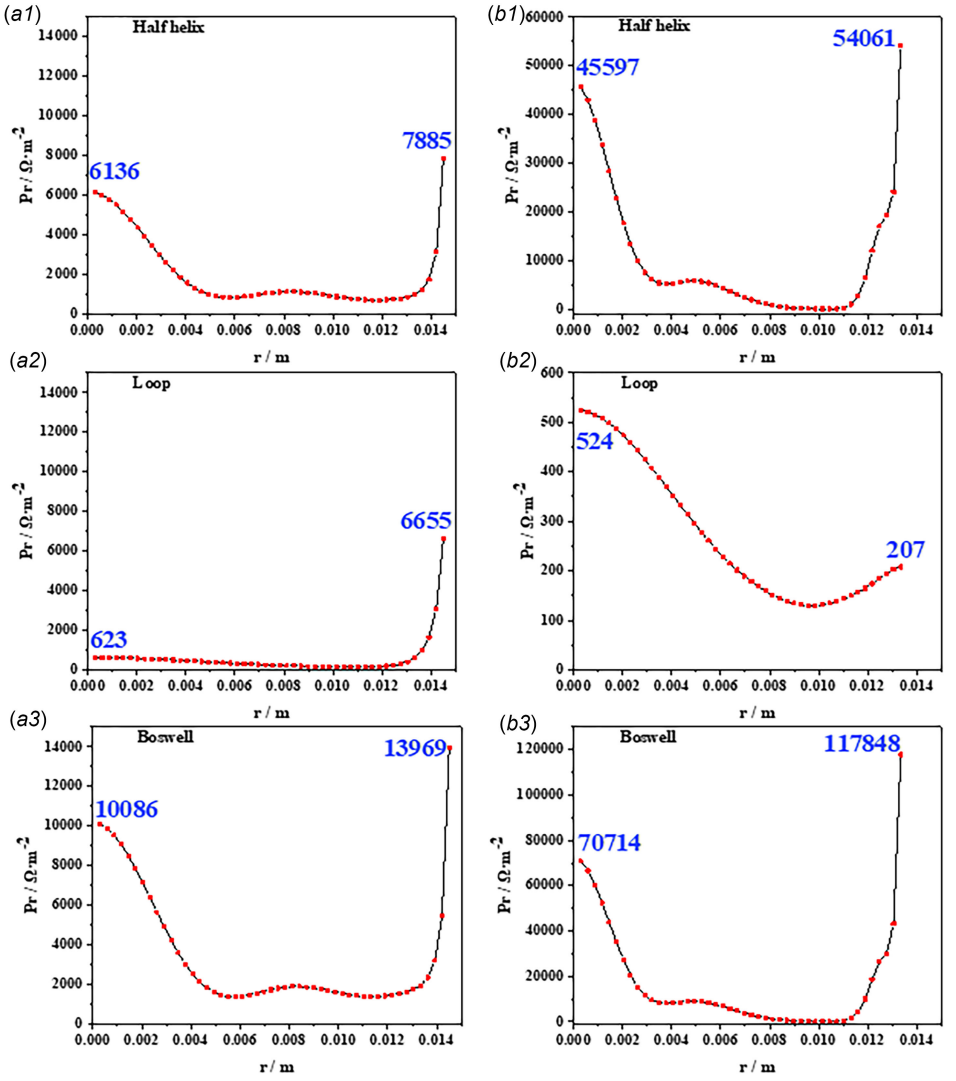


FIGURE 3. Relative absorption power under three types of antennas: (*a*) parabolic distribution; (*b*) Gaussian distribution.

relative absorption power at the centre of the plasma but little difference in relative absorption power at the edge. Since the coupling effect mainly manifests in relative absorption power at the centre, the half-helix antenna can achieve a better coupling effect than the loop antenna. Furthermore, comparing figures 3(*a*1) and 3(*a*3) reveals that the relative absorption power of the Boswell antenna at the plasma centre is numerically higher than that of the half-helix antenna and, correspondingly, the relative absorption power of the Boswell antenna at the edge surpasses that of the half-helix antenna as well. Higher edge relative absorption power indicates more edge heating generation which significantly influences plasma power deposition. Therefore, based on the parabolic distribution, it can be concluded that the half-helix antenna produces superior coupling effect compared to the others.

https://doi.org/10.1017/S0022377825100950 Published online by Cambridge University Press

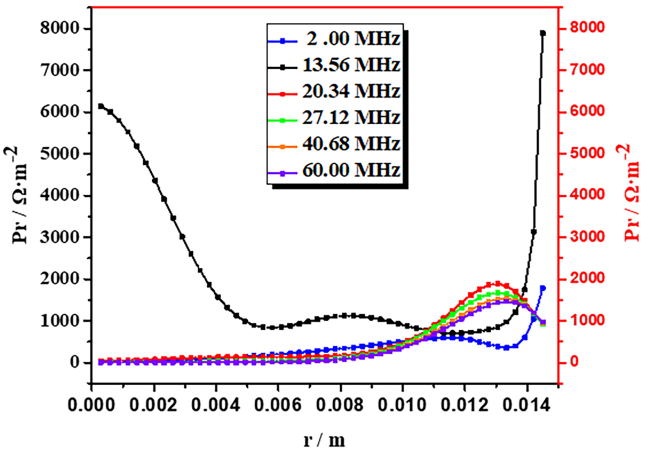


FIGURE 4. Relative absorption power under six RFs. Black axis: 13.56 MHz; red axis: 2, 20.34, 27.12, 40.68 and 60 MHz.

Figures 3(*b*1)–3(*b*3) show the relative absorption power of the half-helix antenna, loop antenna and Boswell antenna under the Gaussian density distribution. The absorption power of the half-helix antenna and Boswell antenna is higher under the Gaussian density distribution compared with the parabolic density distribution, but the overall absorption power distribution is similar. The Boswell antenna exhibits a higher edge relative absorption power than the half-helix antenna, resulting in a decline in the coupling effect. However, the loop antenna with the Gaussian distribution presents a completely different distribution of relative absorption power, possibly due to its two-dimensional nature being affected by different radial density distribution.

Based on the analysis above, it can be concluded that the half-helix antenna can produce better power deposition effects and excite higher plasma density compared with the other two antennas. Therefore, the half-helix antenna is selected as the excitation antenna for HMHX.

3.2. *Radio frequency*

The operating frequency of the antenna is a crucial parameter for HWP discharge, as it directly impacts the power deposition effect between the antenna and plasma. In this study, six common RFs were selected for the HWP discharge, and simulation calculations were conducted to determine the most suitable RFs for HMHX, as shown in figure 4. The black axis corresponds to 13.56 MHz and the red axis corresponds to 2, 20.34, 27.12, 40.68 and 60 MHz.

The results show that the absorption power distribution shows a significant edge enhancement characteristic, and the relative absorption power in the central region is close to zero under the low-frequency condition of 2 MHz. This phenomenon indicates that the helicon wave mode cannot be excited effectively at this frequency, and the discharge is mainly maintained in the inductive coupling mode. It is worth noting that the power absorption curve shows obvious oscillation in the near-edge region, which may be caused by wave mode coupling caused by the low-frequency standing-wave effect. The observed results are consistent with the physical characteristics of the enhanced edge plasma density in a typical ICP discharge. When the frequency is

https://doi.org/10.1017/S0022377825100950 Published online by Cambridge University Press

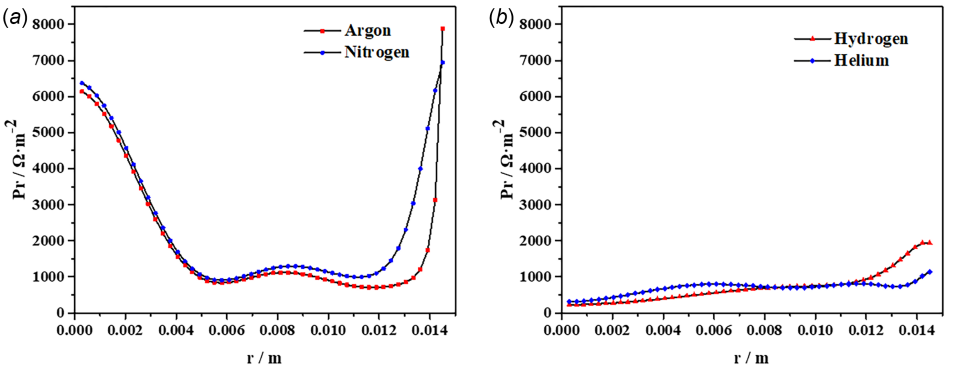


FIGURE 5. Relative absorption power under four types of gas: (*a*) argon and nitrogen; (*b*) hydrogen and helium.

increased to 13.56 MHz, the absorption power distribution changes significantly: the relative absorption power in the central region increases significantly (compared with the 2 MHz condition), while the absorption power in the edge region increases synchronously. The two characteristic parameters show good spatial equilibrium, which indicates that the helical wave dominant discharge mode is successfully excited. The equalisation trend of the spatial distribution confirms that increasing the RF can effectively suppress the inhomogeneity of plasma parameters, which is consistent with the wave field homogenisation effect predicted by spiral wave propagation theory. When the RF continues to increase to 27.12 MHz, the absorbed power in the central region decreases significantly, while the absorption power in the edge region continues to decline. This phenomenon reveals the cutoff effect of electromagnetic wave propagation under high-frequency conditions: when the driving frequency exceeds the critical value, the axial propagation of the spiral wave is strongly inhibited, while the absolute absorption efficiency of the TG wave still decreases with the increase of frequency although it maintains a strong power absorption capacity. This frequency-dependent mode conversion mechanism directly affects the stability of the HWP discharge. Although Chen's research demonstrated that a RF of 27.12 MHz could also achieve HWP discharge mode, the antenna they selected for that frequency was a single-turn annular antenna, and the plasma density generated by its discharge was also lower than that at 13.56 MHz (Chen 2012). In HMHX, the antenna used is a half-helix antenna. The special antenna structure enables it to present the best discharge effect at 13.56 MHz. The results of simulation provide an important theoretical basis for parameter optimisation of HMHX. The follow-up plan is to carry out experimental verification through Langmuir probe diagnosis and emission spectrum diagnosis, focusing on the mode conversion threshold characteristics of the 13.56 MHz band.

3.3. *Gas type*

For HWP discharge, it is necessary to select different gases as discharge gas according to the specific experiment. In common HWP discharge experiments, the selected gases typically include argon, nitrogen, hydrogen and helium. Figure 5 illustrates the radial relative absorption power corresponding to different gases. From figure 5(*a*), it can be observed that when argon and nitrogen are used as discharge

https://doi.org/10.1017/S0022377825100950 Published online by Cambridge University Press

gases, the radial relative absorption power is higher at the centre and edge of the plasma than at other locations. A higher centre absorption power can enhance the power deposition effect of the antenna. However, a higher edge absorption power results in increased temperature at the antenna's edge which will lead to more edge heating due to its own material in the HWP discharge process. Excessive edge heating not only reduces power deposition but also shortens the lifespan of the antenna. Therefore, effective cooling of the antenna itself is crucial during actual discharge experiments. Figure 5(*b*) demonstrates that when using hydrogen and helium as discharge gases, the radial relative absorption power presents a completely different distribution compared with that for argon and nitrogen, with absorption power gradually increasing from centre to edge. While this affects edge heating, it does not allow for higher relative absorption power in the centre which significantly impacts the antenna's power deposition. Without an effective power deposition effect, achieving HWP discharge mode becomes impossible. However, it cannot be denied that in the research of Houshmandyar and Woller, HWP discharge using helium as the discharge gas has been achieved (Houshmandyar, Sears & Thakur 2010; Woller, Whyte & Wright 2017). However, in the experimental research of HMHX, helium discharge has never been achieved, which may be closely related to the structure of the antenna and the parameters of the discharge. In this regard, it is necessary to draw on the experience of other successful discharges and further optimise the device.

To sum up, argon and nitrogen are selected as discharge gases in HMHX to achieve the best power deposition effect. However, due to the strong reducibility of hydrogen, if hydrogen were to be used as a discharge gas to achieve HWP discharge, the higher plasma density will undoubtedly amplify the reducibility of hydrogen in HWP discharge mode, which will have a far-reaching impact on much material processing (Guittienne *et al*. 2021). Therefore, the antenna size will be changed later in this paper to achieve hydrogen–HWP discharge.

3.4. *Parameter optimisation*

To date, many studies have achieved hydrogen–HWP discharge (Lumsdaine, Thakur & Tipton 2020; Caneses Marine *et al*. 2021; Thakur, Simmonds & Caneses 2021). To realise hydrogen–HWP discharge in HMHX, experience can be drawn from these successful cases to better optimise the devices. Firstly, it is essential to optimise the parameters of the helicon wave antenna. When the antenna is a half-helix antenna, and the RF is 13.56 MHz, various sizes of antennas have been chosen for calculation, each corresponding to a different plasma radius. The plasma radius ranges from 6.5 to 22.5 mm at intervals of 2 mm. Figure 6 illustrates how the relative absorption power at the centre and edge of the plasma varies with the plasma radius. During HWP discharge experiments, higher absorption power at the centre can enhance the power deposition effect of both the antenna and plasma. Conversely, higher power absorption at the edge will result in increased edge heating, leading to an uneven radial energy distribution within the plasma and ultimately reducing overall power deposition efficiency. Therefore, when designing a HWP source, it is crucial to avoid generating high relative absorption power at the edge.

The relative absorption power in the central region represented by the black curve presents a typical single-peak distribution with the change of plasma radius. When the plasma radius gradually increases from 6.5 mm, the absorption power at the centre rises rapidly, reaching a peak value (about 1.3 times the initial value) at

https://doi.org/10.1017/S0022377825100950 Published online by Cambridge University Press

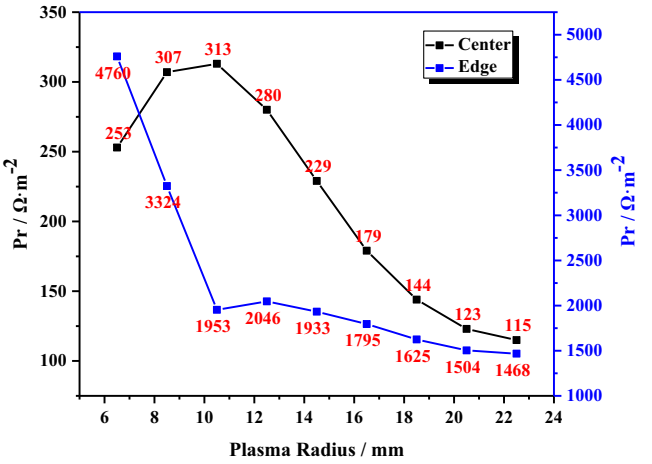


FIGURE 6. Relative absorption power at the centre and edge for different sizes.

$r = 10.5$ mm, and then showing a decreasing trend with the continuing increase of the radius. This phenomenon shows that there is an optimal plasma size effect: too small a discharge cavity cannot afford an effective energy coupling, and too large a size leads to increased energy dissipation. In contrast, the relative absorption power of the edge region represented by the blue curve decreases monotonically with the increase of the radius. It is worth noting that in the range of $r < 10.5$ mm, the edge power will decrease sharply with the increase of the radius (the decrease rate is 59 %), and when $r > 10.5$ mm, the decline rate is significantly reduced. This shows that when the plasma radius exceeds the critical threshold, the contribution of the edge effect to the overall power deposition is negligible.

In the HWP discharge experiment, an external static magnetic field is applied to facilitate deep propagation of H waves within the plasma column, resulting in a greater power deposition effect. Different sizes of helicon wave antennas require different magnetic fields to confine various charged particles in the plasma, optimising the effect of the HWP discharge (Magarotto *et al*. 2019). As for the selection of the magnetic field interval, Thakur's research has achieved significant results in the study of magnetic field scanning in HWP discharge. That research indicates that when the magnetic field varies within a range from low to relatively high (400–2400 Gs), a high-density HWP discharge can be achieved (Thakur, Brandt & Cui 2014). In order to obtain the best hydrogen–HWP discharge in HMHX, the results for the half-helix antenna and RF of 13.56 MHz are maintained under the premise of a plasma radius of 10.5 mm, and the magnetic field intensity is changed to determine the best magnetic field. The calculated range for the magnetic field is 200–2000 Gs. The relative absorption power at the centre and edge under varying magnetic fields is shown in figure 7. It can be observed that as the magnetic field intensity increases, the absorption power at the centre initially rises and then declines. At a magnetic field intensity of 1000 Gs, maximum relative absorption power at the centre is achieved, while at the edge, absorption power decreases initially and then increases with increasing magnetic field strength until reaching a minimum value at 1000 Gs. In HWP discharge experiments, greater absorption power at the centre indicates improved power deposition effects, while lower absorption power

https://doi.org/10.1017/S0022377825100950 Published online by Cambridge University Press

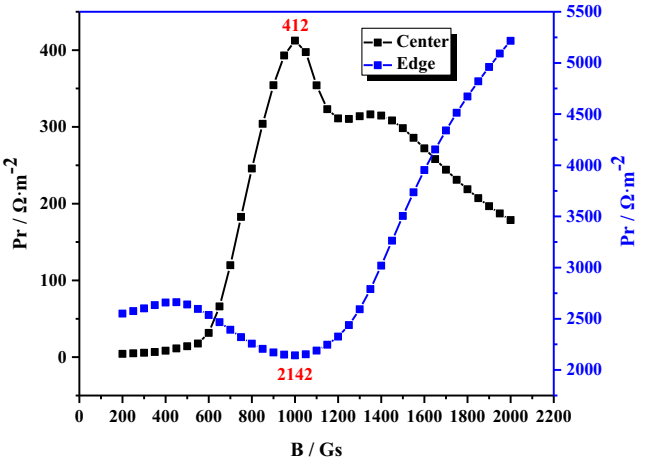


FIGURE 7. Relative absorption power at the centre and edge for different magnetic fields.

at the edge signifies reduced edge heating effects and more uniform energy distribution resulting in better discharge effects. Therefore, both excessively small or large magnetic fields have negative impacts on discharges. For newly designed antennas, optimal discharge effects are achieved when using a magnetic field intensity of 1000 Gs.

4. Conclusions

Using the HELIC code, this study focuses on the parameter optimisation design of a HWP source and compares the results when the radial density distribution is parabolic and Gaussian.

The findings indicate that the half-helix antenna can generate a more effective power deposition and excite higher plasma density compared with the loop antenna and Boswell antenna. Additionally, it is observed that as the RF increases from 2 to 13.56 MHz, the HWP discharge achieves better power deposition effects. However, as the frequency continues to increase beyond 13.56 MHz, there is a gradual decrease in relative absorption power at both the edge and centre of the plasma, with a more significant decrease at the centre. When argon and nitrogen are used as discharge gases, higher centre absorption power can enhance the power deposition effect of the antenna. It is crucial to effectively cool the antenna to mitigate edge heating resulting from higher edge absorption power. Therefore, for HMHX, we recommend using a half-helix antenna as an excitation antenna with a frequency of 13.56 MHz as its power source while utilising argon and nitrogen as discharge gases.

In order to achieve hydrogen–HWP discharge, different sizes of antennas are considered for calculation purposes. When considering relative absorption powers at both the centre and edge, an optimal design consists of an antenna with a plasma radius of 10.5 mm and an overall radius of 13.5 mm. Furthermore, it is noted that different magnetic fields are required for various sizes of helicon wave antennas in order to confine charged particles within the plasma effectively. Too small or too large a magnetic field will have adverse effects on discharge performance. For newly designed antennas targeting hydrogen–HWP discharge applications, it has

https://doi.org/10.1017/S0022377825100950 Published online by Cambridge University Press

been determined that achieving optimal discharge effects requires a magnetic field intensity of 1000 Gs.

The results indicate that different types of HWP discharge experiments can be conducted by designing various sizes of HWP sources. We can carry out hydrogen–HWP discharge experiments using the new antenna based on parameters obtained in this paper to verify the accuracy of calculated results. Additionally, these findings can serve as a reference for optimising existing HWP sources and designing future HWP sources.

Acknowledgements

Editor Troy Carter thanks the referees for their advice in evaluating this article.

Funding

This work was supported by the National Natural Science Foundation of China (grant numbers 12175160, U2341250, 12305284); the National Key R&D Program of China (grant number 2022YFE03050001); and the Priority Academic Program Development of Jiangsu Higher Education Institutions (grant number PAPD).

Declaration of interests

The authors report no conflict of interest.

REFERENCES

ARNUSH, D. & CHEN, F.F. 1998 Generalized theory of helicon waves. II. Excitation and absorption. *Phys. Plasmas* **5**, 1239.

BAKEEV, I.Y., KLIMOV, A.S., OKS, E.M. & ZENIN, A.A. 2023 Operation features of a nonself-sustained glow discharge in a tube initiated by a focused electron beam in the forevacuum pressure range. *IEEE Trans. Plasma. Sci.* **51**, 1941–1945.

BATISHCHEV, O.V. 2009 Minihelicon plasma thruster. *IEEE Trans. Plasma Sci.* **37**, 1563.

CANESES MARIN, J.F. *et al.* 2021 Characterizing the plasma-induced thermal loads on a 200 kW light-ion helicon plasma source via infra-red thermography. *Plasma Sources Sci. Technol.* **30**, 075022.

CARTER, M.D. *et al.* 2022 Comparing experiments with modeling for light ion helicon plasma sources. *Phys. Plasmas* **9**, 5097.

CHANG, L. *et al.* 2024 Research progress and remarks on helicon plasma: a report on the second helicon plasma physics and applications workshop. *Rev. Mod. Plasma Phys.* **8**, 32.

CHANG, L., CANESES, J.F. & THAKUR, S.C. 2022 Wave propagation and power deposition in blue-core helicon plasma. *Front. Phys.* **10**, 9563.

CHANG, L. *et al.* 2018 Coupling of RF antennas to large volume helicon plasma. *Aip Adv.* **8**, 045016.

CHARLES, C. 2009 Topical review: plasmas for spacecraft propulsion. *J. Phys. D: Appl. Phys.* **42**, 163001.

CHARLES, C., BOSWELL, R.W. & LIEBERMAN, M.A. 2003 Energy balance in a low pressure capacitive discharge driven by a double-saddle antenna. *Phys. Plasma* **10**, 891–899.

CHEN, F.F. 2012 Performance of a permanent-magnet helicon source at 27 and 13 MHz. *Phys. Plasma.* **19**, 093509.

CHEN, F.F. 2015 Helicon discharges and sources: a review. *Plasma Sources Sci. Technol.* **24**, 014001.

CHEN, Y. *et al.* 1998 Plasma assisted molecular beam epitaxy of ZnO on c-plane sapphire: growth and characterization. *J. Appl. Phys.* **54**, 3912.

CHI, K.K., SHERIDAN, T.E. & BOSWELL, R.W. 1999 Resonant cavity modes of a bounded helicon discharge. *Plasma Sources Sci. Technol.* **8**, 421.

CUI, R.L. *et al.* 2024 The wave mode transition of argon helicon plasma. *Plasma Sources Sci. Technol.* **33**, 025021.

https://doi.org/10.1017/S0022377825100950 Published online by Cambridge University Press

D'LPPOLITO, D.A. *et al.* 2012 Effect of parallel currents on drift-interchange turbulence: comparison of simulation and experiment. *Phys. Plasma* **19**, 102301.

ELLINGBOE, A.R. & BOSWELL, R.W. 1996 Capacitive, inductive and hellicon-wave modes of operation of a helicon plasma source. *Phys. Plasma* **3**, 2797.

GALLO, A. *et al.* 2017 Impact of the plasma geometry on divertor power exhaust: experimental evidence from TCV and simulations with soledge2D and TOKAM3X. *Plasma Phys. Control. Fusion* **60**, 014007.

GOULDING, R.H. *et al.* 2017 Progress in the development of a high power helicon plasma source for the materials plasma exposure experiment. *Fusion Sci. Technol.* **72**, 588.

GUITTIENNE, P. *et al.* 2021 Helicon wave plasma generated by a resonant birdcage antenna: magnetic field measurements and analysis in the raid linear device. *Plasma Sources Sci. Technol.* **30**, 075023.

HONG, R. *et al.* 2018 Generation of parasitic axial flow by drift wave turbulence with broken symmetry: Theory and experiment. *Phys. Plasma* **25**, 055710.

HONG, R. *et al.* 2018 Tracing the pathway from drift-wave turbulence with broken symmetry to the production of sheared axial mean flow. *Phys. Rev. Lett.* **120**, 205001.

HOUSHMANDYAR, S. *et al.* 2010 Measurements of neutral helium density in helicon plasmas. *Rev. Sci. Instrum.* **81**, 10D704.

HUANG, T.Y., JIN, C.G., YANG, Y., WU, X.M., ZHUGE, L.J., WANG, Q.H. & JI, H.T. 2017*a* Control of ion species and energy in high-flux helicon-wave excited plasma using Ar/N_2 gas mixtures. *IEEE Trans. Plasma Sci.* **46**, 895–899.

HUANG, T.Y., JIN, C.G., YU, J., YANG, Y., ZHUGE, L.J., WU, X.M. & SHA, Z.D. 2017*b* One-step synthesis of silicon oxynitride films using a steady-state and high-flux helicon-wave excited nitrogen plasma. *Plasma Chem. Plasma Process* **37**, 1237–1247.

JUNG, H.D. *et al.* 2004 Development of a compact helicon ion source for neutron generators. *Rev. Sci. Instrum.* **75**, 1878.

KUWAHARA, D. *et al.* 2013 Development of very small-diameter, inductively coupled magnetized plasma device. *Rev. Sci. Instrum.* **84**, 103502.

LI, J.C. *et al.* 2020*a* Helicon wave heating and current drivein toroidal plasmas. *Plasma Phys. Control Fusion* **62**, 095013.

LI, W.Q., ZHAO, B. & WANG, G. 2020*b* Effects of electron temperature on energy deposition properties of electromagnetic modes propagating in helicon plasma. *Acta Phys. Sin.* **69**, 215201.

LI, W.Q., ZHAO, B., WANG, G. & XIANG, D. 2020 Parametric analysis of mode coupling and liner energy deposition properties of helicon and Trivelpiece-Gould waves in helicon plasma. *Acta Phys. Sin.* **69**, 115201.

LUMSDAINE, A. *et al.* 2020 Testing and analysis of steady-state helicon plasma source for the material plasma exposure eXperiment (MPEX). *Fusion Engg Des.* **160**, 112001.

MAGAROTTO, M., MELAZZI, D. & PAVARIN, D. 2019 Study on the influence of the magnetic field geometry on the power deposition in a helicon plasma source. *J. Plasma. Phys.* **4**, 85.

MELAZZI, D. *et al.* 2012 Spires: a finite-difference frequency-domain electromagnetic solver for inhomogeneous magnetized plasma cylinders. *Com. Phys. Comm.* **183**, 1182–1191.

MELAZZI, D. & LANCELLOTTI, V. 2015 A comparative study of radiofrequency antennas for helicon plasma sources. *Plasma Sources Sci. Technol.* **24**, 25024.

MOUZOURIS, Y. & SCHARER, J.E. 1996 Modeling of profile effects for inductive helicon plasma sources. *IEEE Trans. Plasma. Sci.* **24**, 152–160.

PING, L.L. *et al.* 2019 Optimal design of helicon wave antenna and numerical investigation into power deposition on helicon physics prototype experiment. *Acta Phys. Sin.* **68**, 205201.

SHAMRAI, K.P. 1998 Stable modes and abrupt density jumpsin a helicon plasma source. *Plasma Sources Sci. Technol.* **7**, 499–511.

SHINOHARA, S. 2018 Helicon high-density plasma source:physics and applications. *Adv. Phys. X* **3**, 1420424.

SHINOHARA, S. *et al.* 2014 Development of electrodeless plasma thrusters with high-density helicon plasma sources. *IEEE Trans. Plasma. Sci.* **42**, 1245.

SHINOHARA, S. & TANIKAWA, T. 2004 Development of very large helicon plasma source. *Rev. Sci. Instrum.* **74**, 1941.

https://doi.org/10.1017/S0022377825100950 Published online by Cambridge University Press

SHINOHARA, S. & TANIKAWA, T. 2005 Characteristics of a large volume, helicon plasma source. *Phys. Plasma.* **12**, 044502.

SUN, Z.T. *et al.* 2018 Numerical study on an atmospheric pressure helium discharge propagating in a dielectric tube: influence of tube diameter. *Plasma Sci. Phys.* **20**, 7.

TAKAHASHI, K. 2019 Helicon-type radiofrequency plasma thrusters and magnetic plasma nozzles. *Rev. Modern. Plasma. Phys.* **3**, 3.

TANIKAWA, T. & SHINOHARA, S. 2006 Plasma performance in very large helicon device. *Thin Solid Films* **559**, 506–507.

THAKUR, S.C. *et al.* 2014 Multi-instability plasma dynamics during the route to fully developed turbulence in a helicon plasma. *Plasma Sources Sci. Technol.* **23**, 044006.

THAKUR, S.C. *et al.* 2015 Formation of the blue core in argon helicon plasma. *IEEE Trans. Plasma Sci.* **43**, 2754.

THAKUR, S.C. *et al.* 2021 PISCES-RF: a liquid-cooled high-power steady-state helicon plasma device. *Plasma Sources Sci. Technol.* **30**, 055014.

THAKUR, S.C. *et al.* 2013 Suppression of drift wave turbulence and zonal flow formation by changing axial boundary conditions in a cylindrical magnetized plasma device. *Phys. Plasma.* **20**, 012304.

VAEZI, P. *et al.* 2017 Validation study of a drift-wave turbulence model for CSDX linear plasma device. *Phys. Plasma* **24**, 092310.

VAEZI, P. *et al.* 2017 Understanding the impact of insulating and conducting endplate boundary conditions on turbulence in CSDX through nonlocal simulations. *Phys. Plasma* **24**, 042306.

WANG, S.J. *et al.* 2017 Helicon wave coupling in KSTAR plasmas for off-axis current drive in high electron pressure plasmas. *Nucl. Fusion* **57**, 046010.

WOLLER, K.B., WHYTE, D.G. & WRIGHT, G.M. 2017 Broad ion energy distributions in helicon wave-coupled helium plasma. *Phys. Plasma* **24**, 053513.

YEROKHIN, A.L. *et al.* 1999 Plasma electrolysis for surface engineering - sciencedirect. *Surf. Coat. Technol.* **122**, 73.

ZHOU, Y., HUANG, T.Y. & WU, X.M. 2024 Influence of temperature and pressure gradient on power deposition and field pattern in high magnetic field helicon eXperiment. *Contrib. Plasma Phys.* **64**, E202300124.

ZHOU, Y., JI, P.Y., LI, M.Y., ZHUGE, L.J. & WU, X.M. 2023 Influence of magnetic field on power deposition in high magnetic field helicon eXperiment. *Chin. Phy. B* **32**, 025205.

https://doi.org/10.1017/S0022377825100950 Published online by Cambridge University Press